Volume 15, Issue 4, 152424 (1-8)

International Journal of Industrial Chemistry (IJIC)

https://dx.doi.org/10.57647/j.ijic.2024.1504.24

The role of Fe-N_x/N/V_3C_2 nanoelectrocatalyst based on organometallic framework in oxygen reduction activity

Mahdi Soleimani Moghaddam[1], Leila Asadi Kafshgari[2], Mahdieh Houshani[3], Ali Bahari[1,*], Babak Sadeghi[3], Sogol Motallebi Tala Tapeh[3], Ebrahim Shokraei[1]

[1]*Department of Solid-State Physics, Faculty of Science, University of Mazandaran, Babolsar, Iran.*
[2]*Department of Chemical Engineering, Babol Noshirvani University of Technology, Babol, Iran.*
[3]*Departments of Biology & Chemistry, Faculty of Science, Islamic Azad University of Tonekabon, Tonekabon, Iran.*

[*]**Corresponding author:** a.bahari@umz.ac.ir

Research article

Received:
23 July 2024
Revised:
14 August 2024
Accepted:
8 October 2024
Published online:
30 November 2024

Abstract:

In the contemporary era, it is imperative to advance the creation of supremely efficient electrocatalysts for the oxygen reduction reaction (ORR) that utilize readily available, frequent, and economically viable elements. Organometallic frameworks (MOFs), which have the ability to adjust the pore size, have been considered in various research fields, including catalysts. Significantly, a considerable array of materials derived from or founded on MOFs have been utilized for ORR as a result of their expansive surface area, adjustable components, and manageable pore size. In this research, the novel material Fe-N_x/N/V_3C_2 was prepared using a straightforward synthesis method. V_3C_2, when utilized as a conductive substrate, has the capability to hinder the degradation and buildup of the Fe-N-C structure during the pyrolysis process, thereby providing stabilization to the electrocatalyst. The cooperative interactions between Fe-N_x and the V_3C_2 substrate enhance the electron-ion transfer mechanism within the nanocomposite, ultimately establishing a four-electron pathway. Finally, due to the uniform dispersion of Fe-N_x on the V_3C_2 porous substrate, the electrode produced from the nanocomposite showed good ORR catalytic activity with limiting current density (J_D), half-wave potential ($E_{1/2}$) and n values of 4.5 mA cm^{-2}, 0.896 V and 3.98, respectively.

Keywords: Organometallic framework; Fe-N_x/N/V_3C_2; Electrocatalyst; Oxygen reduction

Introduction

Recent major environmental and energy concerns have prompted worldwide endeavors to investigate sustainable energy technologies, including metal-air batteries and fuel cells. Efficient electrocatalysts are necessary for the effective development of these electrochemical devices in order to enhance the activity of the oxygen reduction reaction (ORR) [1–4]. At present, noble metals (e.g., Pt, Ir, Pd) and their alloys have been extensively explored as cathode catalysts for the ORR, while these electrocatalysts seem as sophisticated [5–7]. Specifically, the control of size and morphology offers favorable surface area and noble metal utilization, and the control of composition provides favorable electronic structure effect and synergistic enhancement effect [8]. Nevertheless, the extensive utilization of these applications has been significantly curtailed as a result of restricted resources, exorbitant expenses, and inadequate long-term viability. Hence, it is crucial to design electrocatalysts for ORR that are highly active and composed of materials that are readily available, abundant, and cost-effective. Nowadays, iron-nitrogen-carbon (Fe-N-C) catalysts, which contain FeN_x moieties as catalytic sites, are appealing substitutes for noble metal counterparts among the available possibilities [9]. The quantity of accessible FeN_x sites and the enhancement of their intrinsic activity are crucial for ensuring the ORR efficiency of Fe-N-C electromaterial. For instance, Guo and co-workers [10] illustrated that the com-

bined action of a polyatom and Fe-N-C catalyst has synergistic effects, resulting in enhanced oxygen reduction reaction (ORR) activity and increased electronic structure of the catalyst. Furthermore, certain FeN_x active sites are consistently enclosed within the electrocatalyst's structure in the pyrolysis process, rendering them unreachable to oxygen [11]. A productive strategy involves creating Fe-N-C electrocatalysts that have a high number of mesopores. This helps to enhance use of the active sites of FeN_x and thus enhances the efficiency of the ORR.

Organometallic frameworks (MOFs), known for their pore size adaptability, have been extensively studied in diverse study domains such as separation, adsorption, gas storage, electrocatalysts, and medicines [12–16]. Significantly, a considerable quantity of materials produced from or based on MOFs have been utilized for ORR as a result of their extensive surface area, adjustable constituents, controllable composition, and highly porous structure [17, 18]. The numerous porosity channels present in electrocatalysts formed from MOFs or based on MOFs can offer a higher number of active sites for electrocatalytic activity. This presents significant prospects for creating highly efficient Fe-N-C electrocatalysts. Nevertheless, electrocatalysts generated from MOF, such as Fe-N-C compositions, consistently exhibit suboptimal electrochemical performance as a result of inadequate charge conductivity stemming from the limited level of carbon graphitization [19]. When graphene and carbon nanotubes have been utilized alongside MOFs, their non-polarized carbon surface prevents them from establishing intimate contact with MOFs and effectively modulating the electrical structure of the active sites. Hence, the objective is to identify a substrate that can provide substantial strength in combination with MOFs and effectively modify the electronic structure of the active sites so that the ORR of Fe-N-C electrocatalysts derived from MOFs has a more suitable performance [20, 21].

MXenes are a new type of two-dimensional layered materials that exhibit notable characteristics such as high stability, large surface area, favorable hydrophilicity, and excellent conductivity. It is known that the interaction between polar functional groups in MXenes (e.g., –F and –OH) and water molecules prompts its hydrophilicity. These properties make them intriguing candidates for catalytic studies [22–26]. These classes are commonly synthesized by selectively etching the layer of a double-phase MAX compound, and its chemical formula is typically expressed as $M_{n+1}X_nT_x$, where 'M_{n+1}' signifies an early transition metal, and 'X_n' embodies carbon, nitrogen, boron, and quite recently, oxygen; 'T_x' also denotes surface terminations [27–29]. The common MXenes prepared by etching with HF or HCl and LiF generally have negatively-charged functional groups on their surface (such as -Cl, -F, -O, and -OH). Given the presence of negatively-charged functional groups on their surface, MXenes have negative charged. To instance, Ti_2CT_x is negatively charged with a zeta potential of -32.3 mV [30–32]. Moreover, the presence of a negatively charged on the surface of MXenes creates an appropriate surface for the strong attachment of ions of metal. Therefore, the integration of MXenes with MOFs has the potential to improve the electrocatalytic efficiency of Fe-N-C catalysts produced from MOFs [33].

In this work, $Fe\text{-}N_x/N/V_3C_2$ electrocatalyst was fabricated via an easy and novel method. V_3C_2 serves as a substrate with conductive properties that effectively hinder the degradation and accumulation of the Fe-N-C structure in the process of pyrolysis. This characteristic contributes to the overall stability of the electrocatalyst. To demonstrate this approach, we utilized a MOF called NH_2-MIL-53 that contains iron (Fe) as a starting material to synthesize an iron-based catalyst for the ORR process. The NH_2-MIL-53(Fe) compound contains several porous channels, resulting in a significant increase in surface area and a greater number of accessible active sites.

To enhance the presence of active sites in the $Fe\text{-}N_x$ and prevent the development of metallic iron NPs, iron carbides, or iron oxides, urea was mixed with the suspension prior to carbonization due to contain numerous Fe sites and inadequate nitrogen in MOF. Accordingly, in an alkaline environment, the $Fe\text{-}N_x/N/V_3C_2$ electrocatalyst reveals an outstanding ORR performance that may even surpass Pt/C catalyst.

Materials and methods

Chemicals

Lithium fluoride $\geq$ 99.99%, iron chloride 98%, 2-Aminobenzene-1,4-dicarboxylic acid (NH_2-BDC 99%), sulfuric acid (H_2SO_4 99.99%), urea ($NH_2CONH_2 \geq 99.5\%$), dimethylformamide (DMF, $\geq$ 99.8%), methanol $\geq$ 99.8%, and ethanol (analytical grade), were supplied from Sigma-Aldrich. Moreover, vanadium aluminum carbide (V_3-AlC_2 powder) was obtained from Forsman Scientific Co., Inc. (Beijing, China).

Fabrication of MXene vanadium carbide (V_3C_2 MXene)

MXene vanadium carbide was prepared from V_3-AlC_2 powders by selectively etching Al layers. 1.56 g of lithium fluoride was mixed with 20 mL of during distillation. Therefore, V_3-AlC_2 powder (1 g) was slowly added to the solution, and it was kept at ambient temperature for 2 days. The obtained mixture was centrifuged and rinsed with deionized water several times. Ultimately, the multilayer V_3C_2 MXene was produced using a drying process at a temperature of 60 °C for a duration of 12 hours.

Fabrication of NH_2-MIL-53(Fe)/V_3C_2 MXene

0.2 g of pre-prepared multilayer V_3C_2 MXene was mixed with a solution of DMF (36 mL). The resulting solution was subjected to ultrasonication at room temperature for a duration of 2 hours, leading to its transformation into nanosheets after layering. 1.08 g of iron chloride and 0.77 g of NH_2-BDC were mixed with the mixture mentioned above and agitated for a duration of 1 hour. Then, the mixture was maintained in the hydrothermal reactor for 24 hours at 150 °C. Following the process of cooling to ambient temperature, the prepared product underwent washed with methanol and DMF using centrifugation. Subsequently, the sample was dried at a moderate temperature. The NH_2-MIL-53(Fe) sample was synthesized using similar precursors but without the inclusion of V_3C_2 MXene [33].

Fabrication of Fe-$N_x/N/V_3C_2$

To create more active sites for iron elements, before pyrolysis, 5 g of urea were added to NH_2-MIL-53(Fe)/V_3C_2 powder. Next, the compound was calcined at a heating rate of 5 °C/min under argon flow at 800 °C for 4 hours. After these presses, the black powders were placed in half molar diluted H_2SO_4 at 80 °C for 12 hours to eliminate unstable and inactive components. The ultimate Fe-$N_x/N/V_3C_2$ electromaterial was procured following thorough rinsing with deionized water and subsequent drying at a temperature of 60 °C. To offer a contrast, the Fe-N_x/N sample was prepared by using NH_2-MIL-53(Fe) as a precursor, employing a similar technique. On the other hand, Fe-N_x/V_3C_2 was achieved via directly subjecting NH_2-MIL-53(Fe)/V_3C_2 MXene to pyrolysis without the addition of urea.

Electrochemical measurements

The 3-electrode system includes platinum as the counter electrode, the rotating disk electrode as the working electrode, the Ag|AgCl electrode as the reference, and an electrolyte solution of 0.1 M potassium hydroxide. 0.004 g of catalyst and 25 μL of Nafion are added to 2 mL of ethanol and ultrasonicated for 1 hour, then 5 μL of catalyst ink is loaded on the rotating disc electrode, and after drying, it is ready for testing. Before each test, the electrolyte is exposed to oxygen for 30 minutes.

Results and discussion

The image of the TEM microscope in Fig. 1 showed porous tree-like (hierarchical) sheet nanostructures of Fe-$N_x/N/V_3C_2$. The unique structure of Fe-$N_x/N/V_3C_2$ can be related to the presence of V_3C_2 MXene and urea, which serve as a framework to prevent the clustering and disintegration of MOFs while also producing gas to create various pores. Furthermore, the map analysis of Fe-$N_x/N/V_3C_2$ for elemental distribution studies, reveals that the elements O, C, Fe, and N are evenly dispersed throughout the catalyst's framework. Thus, the bulk form of vanadium in the picture may be due to the boundary atoms of vanadium placed on V_3C_2 MXene, which are thermodynamically semi-stable. The EDS analysis shows the constituent elements of the nanostructure and their atomic and weight percentages and indicates the successful synthesis of the nanocomposite (Table 1). Figures 2A, B present the scanning electron microscope (SEM) images for Fe-$N_x/N/V_3C_2$ hybrid at both low- and high-magnification, which display the size and morphology of the sample. It reveals that the Fe-$N_x/N/V_3C_2$ shows tree-like structure with a uniformity.

Table 1. EDS analysis of the nanocomposite.

ELT	W%	A%
C	8.93	26.08
O	10.51	22.90
N	29.85	32.65
Fe	21.30	9.25
V	29.41	9.12

The XRD pattern of Fe-$N_x/N/V_3C_2$ sample after pyrolysis (etched by LiF for 2 days) is shown in Fig. 3A. As shown in Fig. 3A, V_3C_2 exhibits two peaks at 2θ of 8.7° and 16° corresponding to the (002) and (004) planes in the exfoliated layers [34–36]. Moreover, a significant graphite carbon plane (002) peak can be observed at 25.6°, indicating a highly graphitized structure [37, 38].

Surface analysis by the Brunauer–Emmett–Teller (BET) method is highlighted with isotherms of nitrogen (N_2) absorption/desorption and Barrett–Joyner–Halenda (BJH) pore size distribution as an inset of Fig. 3B for Fe-$N_x/N/V_3C_2$. The obvious hysteresis loop between adsorption and desorption branches could be observed at relative pressure scope of 0.4 – 1.0 for nanocomposite in Fig. 3B, which demonstrated the existence of mesopores. Moreover, BET analysis suggests the high specific surface area of 87 m^2/g with a magnitude of 8 nm for mean pore diameter.

To investigate the ORR catalytic activity of commercial platinum and Fe-$N_x/N/V_3C_2$ and to identify the kinetics of the ORR reaction, linear sweep voltammetry curves were calculated for the nanostructure and other materials synthesized at 1600 s. As it is clear from Fig. 4(A), nanocomposite has a higher threshold potential and half-wave potential compared to other synthesized materials and even commercial platinum, and this indicates the better

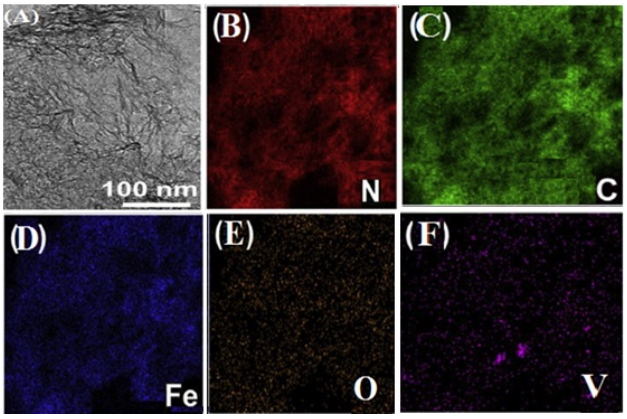

Figure 1. (A) TEM of the Fe-$N_x/N/V_3C_2$ nanocomposite; EDS color mapping of (B) N, (C) C, (D) Fe, (E) O, (F) V in the nanocomposite.

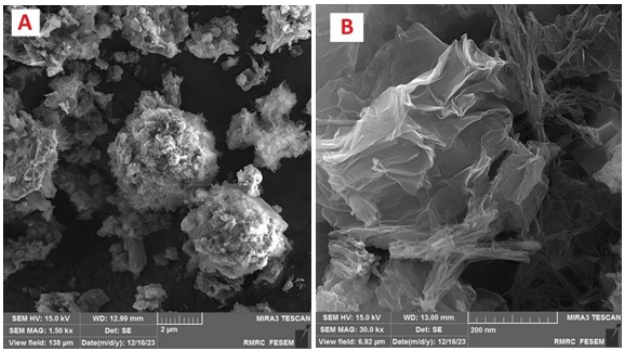

Figure 2. SEM of the Fe-$N_x/N/V_3C_2$ nanocomposite at (A) Low-magnification, and (B) high-magnification.

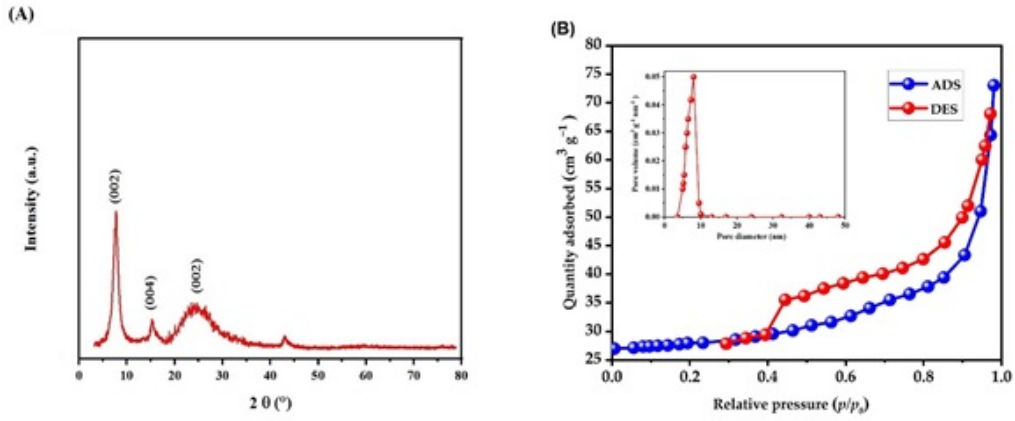

Figure 3. (A) XRD patterns of Fe-N_x/N/V_3C_2; (B) Nitrogen adsorption/desorption isotherms and pore size distributions calculated from N_2 desorption isothermals for Fe-N_x/N/V_3C_2.

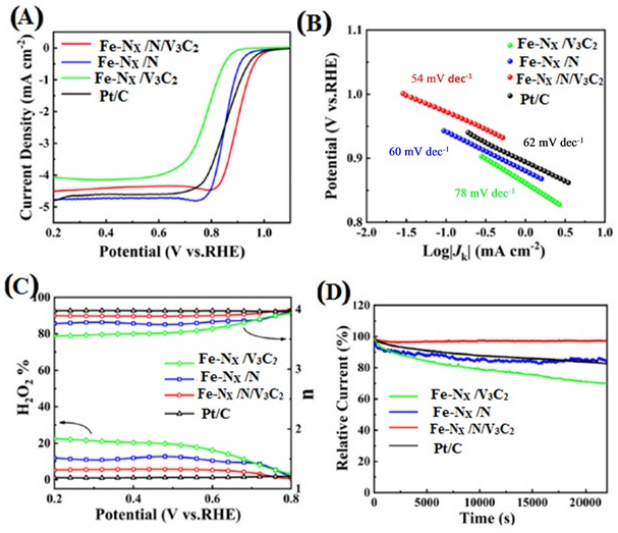

Figure 4. (A) LSV polarization curves of the electrodes; (B) Tafel slope analysis for all electrodes; (C) H_2O_2 production for all electrodes; (D) Chronoamperometric durability test of the samples.

electrocatalytic activity of nanocomposite compared to other synthesized materials. In fact, the peak of cathodic reduction potential for nanocomposite moves towards positive potential compared to other materials and even commercial platinum, which indicates the rapid reduction of the Fe-N_x-O compound and thus better ORR activity. Figure 4(B) shows the evaluation of the additional potential of the Tafel slopes of all samples during the ORR process. Compared to other samples and commercial platinum, the Tafel slope value of nanocomposite is lower, so it can be concluded that nanocomposite has fewer mass transfer limitations compared to others. These findings further verified the exceptional catalytic efficiency of the Fe-N_x/N/V_3C_2 composite in the ORR process.

The production of intermediate species (H_2O_2 or HO_2-) and the number of electrons transported during ORR under the influence of diffusion control can be estimated by using the equations that are given below. These equations are based on ring and disc current values [39].

$$n = \frac{4 \times J_D}{(J_D + \frac{J_R}{N})}$$

$$H_2O_2\% = \frac{100 \times 2 \times \frac{J_R}{N}}{(J_D + \frac{J_R}{N})}$$

$$N = -\frac{J_R}{J_D}$$

The disc current density is denoted as J_D, the ring current density is denoted as J_R, and the rotating ring disk electrode (RRDE) collection efficiency is denoted as N. The value of the number of electrons transported during the ORR, denoted as n, was determined using the equation that relates the disc current density (J_D) with the ring current density (J_R) [40].

Moreover, based on the koutechy-Levich (K-L) schemes (RDE-LSV measurement), we can determine the electron transfer number using the following method:

$$\frac{1}{J} = \frac{1}{J_K} + \frac{1}{B\omega^{1/2}}$$

$$B = 0.2nF(D_0)^{\frac{2}{3}}\upsilon^{-\frac{1}{6}}C$$

The variables in these equations are as follows: ω represents the angular rotation, J stands for measured current density, J_K represents the kinetic current density, and F signifies the Faraday constant ($F = 96485$ C/mol). Oxygen molecules in the alkaline electrolyte have a corresponding diffusion coefficient (D_0) of (1.9×10^{-5} cm^2 s^{-1}) and bulk concentration (C_0) of (1.2×10^{-6} mol cm^{-3}), respectively. kinematic viscosity (0.01 cm^2 s^{-1}) is given by υ. The rotary velocity is measured in rpm by using a fixed value of 0.2. Results indicated that the nanocomposite have good ORR catalytic activity with J_D, half-wave potentials ($E_{1/2}$) and n values of 4.5 mA/cm^2, 0.896 V and 3.98, respectively.

The RRDE test was performed to check the ORR pathway (Fig. 4(C)). According to the calculations, the amount of hydrogen peroxide produced is less than 7%, and the electron transfer path in this electrocatalytic composite is carried out according to the four-electron path. The presence of Fe-N_x and the substrate in the Fe-N_x/N/V_3C_2 composite facilitates the electron-ion transfer process, resulting in an

Table 2. Comparison of the ORR activity of the Fe-N_x/N/V_3C_2 hybrid against other reported ORR catalysts.

ORR catalysts	Half-wave potential, $E_{1/2}$ (V)	J_{limit} (mA/cm^2)	Ref.
Fe-N_x/N/V_3C_2	0.896	4.5	This work
porous dendritic PtNi nanocrystals	0.89	1.76	[41]
PtNi hollow nanochain	0.856	0.48	[42]
Pt_3Ni Polyhedral	0.89	1.43	[43]
Fe-N-C catalyst	0.81	4.31	[44]
FeCo-NP (1000A900)	0.77	-5.56	[45]
$Pt_{1.4}Ni$ tetrapods	0.948	2.01	[46]

enhanced reaction rate of the Fe-N_x/N/V_3C_2 electrocatalyst due to synergistic effects. Furthermore, the oxygen molecules exhibit a high propensity for dissociation, ultimately resulting in the formation of a four-electron route within the Fe-N_x/N/V_3C_2 composite.

As shown in Fig. 4(D), after 6 hours of operation, the stability comparison of the nanocomposite and commercial platinum confirmed that the nanocomposite maintains 96% of its beginning current, while this value is 85% for commercial platinum. The Fe-N_x/N/V_3C_2 electrocatalyst exhibits superior durability compared to the other commercially available platinum (Table 2) [41–46]. The uniform dispersion of Fe-N_x on the substrate is due to the effective role of the electrocatalyst substrate and its highly porous structure. This ensures that the nanocomposite remains stable and reliable for a long period of time throughout the ORR process. Nanocomposite showed good ORR catalytic activity with J_D, $E_{1/2}$ and n values of 4.5 mA cm^{-2}, 0.896 V and 3.98, respectively. Moreover, to study of the stability of the Fe-N_x/N/V_3C_2 hybrid after cycling for ORR, the surface analysis was performed. As can be seen from Fig. 5, morphology changes are very minor and in fact it is unchanged. This fact verifies that the Fe-N_x/N/V_3C_2 hybrid has good stability.

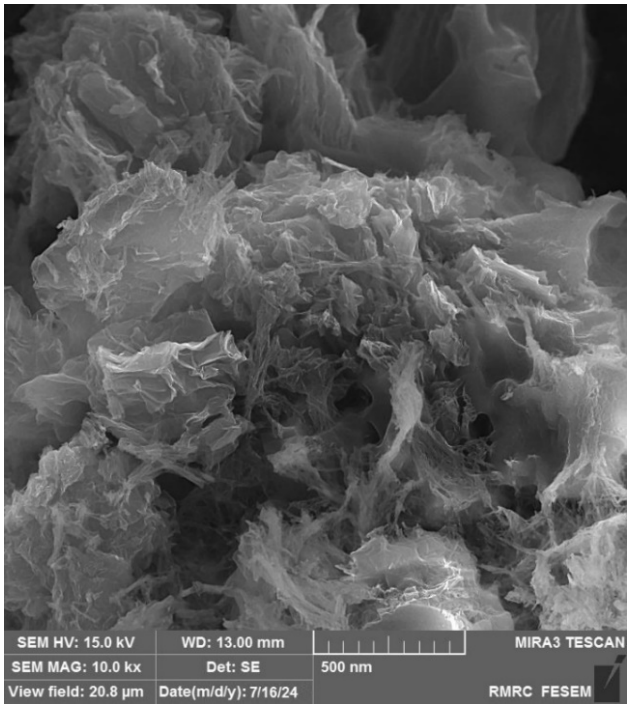

Figure 5. The morphology of the Fe-N_x/N/V_3C_2 hybrid after cycling for ORR.

Conclusion

In this study, Fe-N_x/N/V_3C_2 electrocatalyst was fabricated by a simple and novel method. V_3C_2, functioning as a conductive substrate, have effectively hinder the degradation and accumulation of the Fe-N-C structure while also providing stability to the electrocatalyst through the pyrolysis process. The iron-based MOF, was utilized as a starting material to produce a catalyst in the ORR process. The frequent porous channels within NH_2-MIL-53 (Fe) can ensure a wide surface area and more reachable active sites for Fe-N_x/N/V_3C_2. According to the findings, the Fe-N_x/N/V_3C_2 electrocatalyst exhibits exceptional ORR efficiency that is comparable to, or even surpasses, that of the Pt/C catalyst in alkaline environments. The presence of Fe-N_x and the substrate in the Fe-N_x/N/V_3C_2 composite facilitates the electron-ion transfer, leading to a boosted reaction rate of the Fe-N_x/N/V_3C_2 electrocatalyst due to synergistic effects. Also, easy separation of oxygen molecules created a four-electron pathway for nanocomposite. Finally, the Fe-N_x/N/V_3C_2 electrocatalyst indicated more durability than the commercial platinum catalyst. The uniform scattering of Fe-N_x on the V_3C_2 substrate is due to the effective role of the electrocatalyst substrate and its very porous structure, which guarantees the long-term and significant stability of the nanocomposite during the ORR process.

Authors contributions
All authors have contributed equally to prepare the paper.

Availability of data and materials
The data that support the findings of this study are available from the corresponding author upon reasonable request.

Conflict of interests
The authors declare that they have no known competing financial interests or personal relationships that could have appeared to influence the work reported in this paper.

References

[1] S. D. Bhoyate, J. Kim, F. M. de Souza, J. Lin, E. Lee, A. Kumar, et al. "Science and engineering for non-noble-metal-based electrocatalysts to boost their ORR performance: A critical review.". *Coordination Chemistry Reviews*, **474**:214854, 2023.

[2] I. Muthuvel, K. Gowthami, G. Thirunarayanan, P. Suppuraj, B. Krishnakumar, A. J. F. do Nascimento Sobral, et al. "Graphene oxide–$Fe_2V_4O_{13}$ hybrid material as highly efficient hetero-Fenton catalyst for degradation of methyl orange.". *International Journal of Industrial Chemistry*, **10**:77–87, 2019.

[3] A. C. V. Olivares, M. F. Gomez, M. N. Barroso, and M. C. Abello. Ni-supported catalysts for ethanol steam reforming: effect of the solvent and metallic precursor in catalyst preparation. *International Journal of Industrial Chemistry*, **9**:61–73, 2018.

[4] A. H. Abdel Aziz, T. S. Jamil, M. S. Shalaby, A. M. Shaban, E. R. Souaya, and N. A. Abdel Ghany. Application of (polyaniline/zeolite x) composite as anticorrosion coating for energy recovery devices in ro desalination water plants. *International Journal of Industrial Chemistry*, **10**:175–91, 2019.

[5] S. Zhang, W. Xia, Q. Yang, Y. Valentino Kaneti, X. Xu, S. M. Alshehri, et al. Core-shell motif construction: Highly graphitic nitrogen-doped porous carbon electrocatalysts using mof-derived carbon@cof heterostructures as sacrificial templates. *Chemical Engineering Journal*, **396**:125154, 2020.

[6] Z. Yang, M. Xiang, Y. Zhu, J. Hui, Y. Jiang, S. Dong, et al. "Single-atom platinum or ruthenium on C4N as 2D high-performance electrocatalysts for oxygen reduction reaction.". *Chemical Engineering Journal*, **426**:131347, 2021.

[7] R. Verma, I. Chakraborty, S. Chowdhury, M. M. Ghangrekar, and R. Balasubramanian. Nitrogen and sulfur codoped graphene macroassemblies as high-performance electrocatalysts for the oxygen reduction reaction in microbial fuel cells. *ACS Sustainable Chemistry & Engineering*, **8**(44):16591–9, 2020.

[8] H. Wang, S. Yin, Y. Xu, X. Li, A. A. Alshehri, Y. Yamauchi, et al. Direct fabrication of tri-metallic ptpdcu tripods with branched exteriors for the oxygen reduction reaction. *Journal of Materials Chemistry A.*, **6**(18):8662–8, 2016.

[9] S. Akula, M. Mooste, B. Zulevi, S. McKinney, A. Kikas, H.-M. Piirsoo, et al. Mesoporous textured fe-nc electrocatalysts as highly efficient cathodes for proton exchange membrane fuel cells. *Journal of Power Sources*, **520**:230819, 2022.

[10] S. Chen, Y. Yan, P. Hao, M. Li, J. Liang, J. Guo, et al. Iron nanoparticles encapsulated in s, n-codoped carbon: Sulfur doping enriches surface electron density and enhances electrocatalytic activity toward oxygen reduction. *ACS applied materials & interfaces*, **12**(11):12686–95, 2020.

[11] L. Zhao, Y. Zhang, L.-B. Huang, X.-Z. Liu, Q.-H. Zhang, C. He, et al. Cascade anchoring strategy for general mass production of high-loading single-atomic metal-nitrogen catalysts. *Nature communications*, **10**(1):1278, 2019.

[12] M. S. Kafshgari, M. Jahanshahi, and M. Ghorbani. Magnetic coordination polymer for dye removal and antibacterial activity. *Journal of the Taiwan Institute of Chemical Engineers*, **149**:104995, 2023.

[13] H. Hamedani, A. K. Ghasemi, M. S. Kafshgari, Y. Zolfaghari, and L. A. Kafshgari. Electrochemical performance of 3d porous pani/gr/mil-100(fe) nanocomposite as a novel smart supercapacitor electrode material. *Synthetic Metals*, **298**:117428, 2023.

[14] A. Azizi, M. Forghani, L. A. Kafshgari, and A. Hassanzadeh. Adsorptive removal behavior of pb (ii) and cr (vi) pollutants from an aqueous environment onto polyaniline-modified mil100(fe). *Minerals*, **13**(3):299, 2023.

[15] A. Felix Sahayaraj, H. Joy Prabu, J. Maniraj, M. Kannan, M. Bharathi, P. Diwahar, et al. Metal–organic frameworks (mofs): The next generation of materials for catalysis, gas storage, and separation. *Journal of Inorganic and Organometallic Polymers and Materials*, pages 1–25, 2023.

[16] M.-A. Gatou, I.-A. Vagena, N. Lagopati, N. Pippa, M. Gazouli, and E. A. Pavlatou. Functional mof-based materials for environmental and biomedical applications: a critical review. *Nanomaterials*, **13**(15):2224, 2023.

[17] K. Dhanabalan, M. Perumalsamy, G. Sriram, N. Murugan, T. Sadhasivam, and T. H. Oh. Metal–organic framework (mof)-derived catalyst for oxygen reduction reaction (orr) applications in fuel cell systems: A review of current advancements and perspectives. *Energies*, **16**(13):4950, 2023.

[18] J. Li, W. Xia, J. Tang, H. Tan, J. Wang, Y. V. Kaneti, et al. Mof nanoleaves as new sacrificial templates for the fabrication of nanoporous co–n x/c electrocatalysts for oxygen reduction. *Nanoscale Horizons*, **4**(4):1006–13, 2019.

[19] K. F. Tadavani, M. Zhiani, H. Gharibi, and H. B. Dehkordi. Preparation of a high-performance fe-n-c electrocatalyst from an mof precursor for orr toward zinc-air batteries. *Energy & Fuels*, **37**(23):19092–102, 2023.

[20] C. Fang, X. Tang, and Q. Yi. Adding fe/dicyandiamide to co-mof to greatly improve its orr/oer bifunctional electrocatalytic activity. *Applied Catalysis B: Environmental*, **341**:123346, 2024.

[21] J. S. Bates, F. Khamespanah, D. A. Cullen, A. A. Al-Omari, M. N. Hopkins, J. J. Martinez, et al. Molecular catalyst synthesis strategies to prepare atomically dispersed fe-n-c heterogeneous catalysts. *Journal of the American Chemical Society*, **144**(41):18797–802, 2022.

[22] Q. Wang, N. Han, A. Bokhari, X. Li, Y. Cao, S. Asif, et al. Insights into mxenes-based electrocatalysts for oxygen reduction. *Energy*, **255**:124465, 2022.

[23] Sunita, U. Ghanekar, and S. Meena. Heteroatom induced tailoring electronic and optical properties of v_3c_2 mxene through bandgap opening: A computational insight. *Chemical Physics Letters*, **799**:139639, 2022.

[24] Y.-Z. Zhang, J. K. El-Demellawi, Q. Jiang, G. Ge, H. Liang, K. Lee, et al. Mxene hydrogels: fundamentals and applications. *Chemical Society Reviews*, **49** (20):7229–51, 2020.

[25] Z. Wu, T. Shang, Y. Deng, Y. Tao, and Q. H. Yang. The assembly of mxenes from 2d to 3d. *Advanced science*, **7**(7):1903077, 2020.

[26] B. Anasori, M. R. Lukatskaya, and Y. Gogotsi. 2d metal carbides and nitrides (mxenes) for energy storage. *Nature Reviews Materials*, **2**(2):1–17, 2017.

[27] S. Saharan, U. Ghanekar, and S. Meena. "Black phosphorus/V_3C_2 MXene layered heterostructure as a sustainable cathode material for Li-Ion battery: An Ab initio study.". *The Journal of Physical Chemistry C*, **127**(19):8905–12, 2023.

[28] N. Rabiee and S. Iravani. Mxenes and their composites: a versatile platform for biomedical applications. *Materials Chemistry Horizons*, **2**(3):171–84, 2023.

[29] K. Salimiyan Rizi. Mxene nanosheets as a novel nanomaterial with antimicrobial applications: A literature review. *Journal of Molecular Structure*, **1262**:132958, 2022.

[30] X. Wang, J. Wang, J. Qin, X. Xie, R. Yang, and M. Cao. Surface charge engineering for covalently assembling three-dimensional mxene network for all-climate sodium ion batteries. *ACS applied materials & interfaces*, **12**(35):39181–94, 2020.

[31] B. Sun, X. Dong, H. Li, Y. Shang, Y. Zhang, F. Hu, et al. "Surface charge engineering for two-dimensional Ti_2CT_x MXene for highly efficient and selective removal of cationic dye from aqueous solution.". *Separation and Purification Technology*, **272**:118964, 2021.

[32] C.E. Ren, K.B. Hatzell, M. Alhabeb, Z. Ling, K.A. Mahmoud, and Y. Gogotsi. "Charge-and size-selective ion sieving through $Ti_3C_2T_x$ MXene membranes.". *The journal of physical chemistry letters*, **6**(20):4026–31, 2015.

[33] W. Gu, M. Wu, J. Xu, and T. Zhao. Mxene boosted metal-organic framework-derived fe-n-c as an efficient electrocatalyst for oxygen reduction reactions. *International Journal of Hydrogen Energy*, **47**(39):17224–32, 2022.

[34] R. Choudhury, N. Kurra, and P. Meduri. Doped microsilicon and vanadium carbide mxene composite as anode for high stability and high capacity li-ion batteries. *Results in Engineering*, **19**:101338, 2023.

[35] M. Wu, B. Wang, Q. Hu, L. Wang, and A. Zhou. "The synthesis process and thermal stability of V2C MXene. ". *Materials*, **11**(11):2112, 2018.

[36] Z. Li, L. Wang, D. Sun, Y. Zhang, B. Liu, Q. Hu, et al. "Synthesis and thermal stability of two-dimensional carbide MXene Ti_3C_2.". *Materials Science and Engineering: B*, **191**:33–40, 2015.

[37] C. Zeng, Y. Wang, J. Wan, Y. Ma, J. Yi, and S. Zuo. Three-dimensional hollow catalysts with edge-defective fe-nx sites and enhanced peroxymonosulfate activation performance: Preparation, applications, and mechanism. *Separation and Purification Technology*, **325**:124696, 2023.

[38] Z. Yang, X. Zhang, K. Huang, M. Waqas, X. Peng, L. Wang, et al. M–nx–c (m = fe, zn) bi-active sites booting oxygen reduction reaction and zinc-air battery performance. *Journal of Electroanalytical Chemistry*, **967**:118475, 2024.

[39] K. Kisand, A. Sarapuu, J. C. Douglin, A. Kikas, A. Treshchalov, M. Kaarik, et al. Templated nitrogen-, iron-, and cobalt-doped mesoporous nanocarbon derived from an alkylresorcinol mixture for anion-exchange membrane fuel cell application. *Acs Catalysis*, **12**(22):14050–61, 2022.

[40] N. Bhuvanendran, S. Ravichandran, Q. Xu, T. Maiyalagan, and H. Su. quick guide to the assessment of key electrochemical performance indicators for the oxygen reduction reaction: A comprehensive review. *International Journal of Hydrogen Energy*, **47**(11):7113–38, 2022.

[41] K. Eid, H. Wang, V. Malgras, Z. A. Alothman, Y. Yamauchi, and L. Wang. Facile synthesis of porous dendritic bimetallic platinum–nickel nanocrystals as efficient catalysts for the oxygen reduction reaction. *Chemistry-An Asian Journal*, **11**(9):1388–93, 2016.

[42] S. Fu, C. Zhu, J. Song, M.H. Engelhard, Y. He, D. Du, et al. Three-dimensional ptni hollow nanochains as an enhanced electrocatalyst for the oxygen reduction reaction. *Journal of Materials Chemistry A*, **4**(22): 8755–61, 2016.

[43] Y. Liu, H. Chen, C. Tian, D. Geng, D. Wang, and S. Bai. One-pot synthesis of highly efficient carbon-supported polyhedral pt 3 ni alloy nanoparticles for oxygen reduction reaction. *Electrocatalysis*, **10**:613–20, 2016.

[44] Y. Jiang, H. Xu, B. Ma, Z. Zhang, and Y. Zhou. Polypyrrole derived carbon nanotube aerogel based single-site fe-n-c catalyst with superior orr activity and durability. *Fuel*, **366**:131404, 2024.

[45] H.-C. Tu, Y.-L. Hsiao, Y.-D. Lin, Y.-G. Lin, D.-L. Liao, and K.-S. Ho. Multi-functional hydrogen- and oxygen-capturing feco-n-c catalyst with improved hydrogenation of nitroarenes and orr activity. *Chemical Engineering Journal*, **487**:150623, 2024.

[46] L. Chen, N. Cheng, S. Yu, H. Jiang, H. Jiang, and C. Li. "Pt 1.4 Ni (100) Tetrapods with enhanced oxygen reduction reaction activity.". *Catalysis Letters*, **151**:212–20, 2020.